

PORE ROUGHNESS EFFECTS ON HIGH-FREQUENCY PERMEABILITY

David Smeulders and Andrea Cortis

Delft University of Technology, PO Box 5028, 2600 GA, Delft, The Netherlands

d.m.j.smeulders@ta.tudelft.nl

Jean Luc Guermond

LIMSI, UPR 3251 (CNRS), BP 133, 91403 Orsay, France

Denis Lafarge

LAUM, UMR 6613, Av. O. Messiaen, 72017, Le Mans, France

Abstract The high-frequency behaviour of the dynamic permeability is studied. In the case that the solid-fluid interface appears locally flat, we give a new derivation for the characteristic length Λ . In the case of wedge-shaped intrusions, the classical approach is modified by an additional higher-order term, which is depending on the apex angle of the wedge. Precise numerical simulations confirmed this dependency.

Keywords: Dynamic permeability, pore roughness, numerical simulations

Introduction

By definition, the dynamic permeability $k(\omega)$ describes the (linear) response of a simple incompressible fluid in a porous medium subjected to a harmonic pressure drop across the sample. This response has been widely studied before [2, 6, 10], and is involved in many problems and applications. As an example, the dynamic permeability is the fundamental ingredient to describe sound propagation in a fluid-saturated rigid-framed porous medium as long as the wavelength is large compared to the characteristic sizes of pores and grains in the medium. Relaxing the assumption of a rigid frame, the concept may be incorporated in the Biot theory.

Under the assumption that the fluid-solid interface appears locally flat if the viscous skin depth δ is small enough, Johnson et al. [6] obtained the high-

frequency result

$$k(\omega) = \frac{\varepsilon^2 \phi}{\alpha_\infty} (1 - C\varepsilon + \dots). \quad (1)$$

Here, $\varepsilon = \sqrt{\nu/i\omega} = (1 - i)\delta/2$ is the complex viscous skin depth parameter, and ϕ , α_∞ , and C are purely geometrical parameters, respectively the porosity, tortuosity, and $C = 2/\Lambda$, where Λ is a pore size parameter characterizing transport properties of the porous material [6].

We will first clarify the existing discrepancies between the result (1) and the expression by Sheng & Zhou [9]. Next, we will consider a rugged geometry in the form of two-dimensional pore channels with wedge-shaped intrusions (see Fig. 1), and we will show that the high-frequency result becomes

$$k(\omega) = \frac{\varepsilon^2 \phi}{\alpha_\infty} (1 - C\varepsilon - C_w \varepsilon^w + \dots), \quad (2)$$

where the exponent w ($1 < w < 2$) is related to the apex angle γ ($0 < \gamma < \pi$) of the wedges:

$$w = \frac{2\pi}{2\pi - \gamma}. \quad (3)$$

We found that (3) is different from an expression proposed by Achou & Avel-

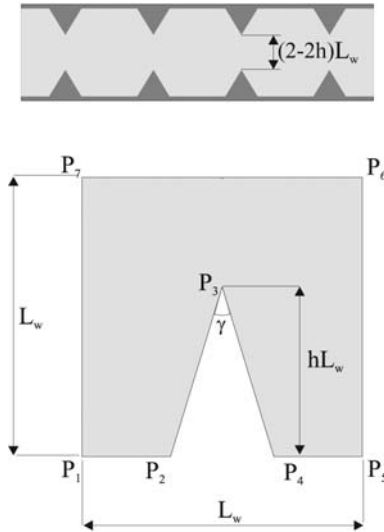


Figure 1. Geometry of the two-dimensional channel with intrusive wedges (top picture). The dimensions of the wedges are drawn at the bottom picture.

laneda [1]. A theoretical study and numerical simulations will show that (3) is the correct expression.

Conceptual Model

We define the scaled velocity field $\tilde{\mathbf{v}}$, which solves the following oscillating Stokes flow problem:

$$\varepsilon^{-2}\tilde{\mathbf{v}} = -\nabla\tilde{p} + \Delta\tilde{\mathbf{v}} + \mathbf{e}, \quad \nabla \cdot \tilde{\mathbf{v}} = 0, \quad (4)$$

where \mathbf{e} is the unit macroscopic pressure gradient. Moreover, we assume that $\tilde{\mathbf{v}} = 0$ on the pore surface S_p , and that \tilde{p} is compact, which means that the field has a constant pore averaged value, i.e., on the average it does not increase or decrease in the direction of \mathbf{e} . The dynamic permeability is, by definition, the direct pore volume average

$$k(\omega) = \frac{\phi}{V_p} \int_{V_p} \tilde{\mathbf{v}} \cdot \mathbf{e} dV. \quad (5)$$

Similarly, we define the scaled potential field \mathbf{E} which solves the potential problem

$$\mathbf{E} = -\nabla\Phi + \mathbf{e}, \quad \nabla \cdot \mathbf{E} = 0. \quad (6)$$

Here, $\mathbf{E} \cdot \mathbf{n} = 0$ on S_p (Neumann type boundary condition), where \mathbf{n} is the unit outward normal from the pore region, and Φ is compact. \mathbf{E} can be interpreted as the microscopic electric field induced in the pore space when a unit macroscopic field \mathbf{e} is applied, assuming insulating solid phase and uniform conductivity in the pore fluid. Its pore volume average is directly related to the tortuosity α_∞ :

$$\frac{1}{\alpha_\infty} = \frac{1}{V_p} \int_{V_p} \mathbf{E} \cdot \mathbf{e} dV. \quad (7)$$

Using integration by parts it is easily verified that for any compact field Φ there is the orthogonality relation

$$\int_{V_p} \mathbf{w} \cdot \nabla\Phi dV = 0, \quad (8)$$

for any divergence-free field \mathbf{w} having zero normal component on the pore surface. Thus, the dynamic permeability and tortuosity may be written in equivalent form:

$$k(\omega) = \frac{\phi}{V_p} \int_{V_p} \tilde{\mathbf{v}} \cdot \mathbf{E} dV, \quad (9)$$

$$\frac{1}{\alpha_\infty} = \frac{1}{V_p} \int_{V_p} E^2 dV. \quad (10)$$

We now consider the high-frequency limit $\varepsilon/L_w \rightarrow 0$ of the scaled field $\tilde{\mathbf{v}}$, where L_w is a characteristic pore size. As argued by [6], the fluid motion

is given by potential flow except for a boundary layer of thickness δ near the pore walls. To leading order, we have $\varepsilon^{-2}\tilde{\mathbf{v}} \rightarrow \mathbf{E}$ and $\tilde{p} \rightarrow \Phi$ in the bulk potential flow region. A more exact replacement would be $\varepsilon^{-2}\tilde{\mathbf{v}} \rightarrow \mathbf{E} - \nabla\Pi$ and $\tilde{p} \rightarrow \Phi + \Pi$, with Π being a small, $\mathcal{O}(\varepsilon)$, compact perturbation induced by the presence of the boundary layer. Assuming that the boundary layer is small enough so that the walls of the pores appear locally flat, the perturbation term may be determined by introducing in the analogous electric conductivity problem a layer of variable conductivity near the pore walls. The variable conductivity is chosen to generate for the current the known variations of the tangential components of the velocity field in the boundary layer. When the pore walls have a non-trivial shape, the divergence-free nature of the current naturally implies the existence of normal components near the pore walls that act as a source for the perturbed potential in the bulk. Following the assumption of locally plane pore walls, the tangential components of the velocity in the boundary layer may be written to leading order [7]

$$\varepsilon^{-2}\tilde{\mathbf{v}} = (1 - e^{-\beta/\varepsilon})\mathbf{E}, \quad (11)$$

where β is a local co-ordinate measured from the pore walls into the bulk of the pore. We thus consider the perturbed potential problem ($\nabla \cdot \tilde{\mathbf{v}} = 0$)

$$\varepsilon^{-2}\tilde{\mathbf{v}} = \sigma(\mathbf{r})(\mathbf{E} - \nabla\Pi). \quad (12)$$

The field $\varepsilon^{-2}\tilde{\mathbf{v}}$ is the current induced when a unit electric field is applied for a medium having insulating solid phase and conductivity $\sigma(\mathbf{r}) = 1 - \exp(-\beta/\varepsilon)$ in the pore region. Current conservation yields:

$$\nabla \cdot (\sigma\nabla\Pi) = \mathbf{E} \cdot \nabla\sigma. \quad (13)$$

In the limit $\varepsilon/L_w \rightarrow 0$, only derivatives normal to the pore walls need to be considered. Straightforward integration yields the following velocity pattern in the boundary layer:

$$\varepsilon^{-2}\tilde{\mathbf{v}} = (1 - e^{-\beta/\varepsilon})\mathbf{E} + \varepsilon\mathbf{n}[1 - (1 + \beta/\varepsilon)e^{-\beta/\varepsilon}] \left(\frac{\partial E_\beta}{\partial \beta} \right)_{\beta=0}. \quad (14)$$

Setting $\beta/\delta \rightarrow \infty$ in (14) and (12), we derive the boundary condition $\partial\Pi/\partial\beta = \varepsilon(\partial E_\beta/\partial\beta)_{\beta=0}$. The velocity field hence determined in the bulk is (Cortis et al. 2003):

$$\varepsilon^{-2}\tilde{\mathbf{v}} = \mathbf{E} + \varepsilon\mathbf{N}, \quad (15)$$

where the perturbation field \mathbf{N} is a purely geometrical vector field, accounting for the presence tangential components in the boundary layer. Now evaluating the integral (5), the first term $\varepsilon^2\phi/\alpha_\infty$ in (1) stems from the leading bulk term

\mathbf{E} in (15) and the constant boundary layer tangential term \mathbf{E} in (14). The second term $(\varepsilon^2\phi/\alpha_\infty)C\varepsilon$ stems from two contributions leading to the new result:

$$\frac{2}{\Lambda} = \frac{\int_{S_p} \mathbf{E} \cdot \mathbf{e} dS}{\int_{V_p} E^2 dV} - \frac{\int_{S_p} \Phi(\partial E_\beta/\partial\beta) dS}{\int_{V_p} E^2 dV}. \quad (16)$$

The first is a boundary layer contribution related to the tangential components $-\exp(-\beta/\varepsilon)\mathbf{E}$ in (14). The second stems from the perturbation field $\varepsilon\mathbf{N}$ [4]. Sheng & Zhou [9] erroneously identified $2/\Lambda$ to be the first term on the right-hand-side of (16), because they used the incomplete replacement $\varepsilon^{-2}\tilde{\mathbf{v}} \rightarrow \mathbf{E}$. Note that in straight pore channels ($\mathbf{E} = \mathbf{e}$) the second contribution vanishes while the first reduces to the pore surface-to-volume ratio S_p/V_p . In general, both contributions are of the same order of magnitude. It can also be shown [4] that (16) can be rewritten as

$$\frac{2}{\Lambda} = \frac{\int_{S_p} E^2 dS}{\int_{V_p} E^2 dV}, \quad (17)$$

which is the classical relation obtained by [6]. A more compact way to derive (16), is to use (9) instead of (5). No bulk contribution arises because of the orthogonality (8) between \mathbf{E} and \mathbf{N} .

Corrugated Pore Channels

As argued by Achdou & Avellaneda [1], a two-dimensional reasoning is sufficient to study the singularity. The periodic geometry is depicted in Fig. 1. The wedge is defined by its apex angle γ . Introducing polar co-ordinates r, θ , we set the origin $r = 0$ on the tip of the wedge and count the angle θ from one side of the wedge. The singular potential field $\mathbf{E}(r, \theta)$ may be written [7]

$$E_r = Anr^{n-1} \cos n\theta \quad E_\theta = -Anr^{n-1} \sin n\theta, \quad (18)$$

where A is an amplitude factor and $\frac{1}{2} < n = \pi/(2\pi - \gamma) < 1$. The contribution of the wedges to the integral (9) may be evaluated noting that the velocity field $\tilde{\mathbf{v}}$ matches to leading order the value $\varepsilon^2\mathbf{E}$ on the bounding surface of the potential flow region. Thus, according to (18), the external potential fields \mathbf{E} and $\tilde{\mathbf{v}}$ must vary like ε^{n-1} and ε^{n+1} , respectively, when integrating in the boundary layer around the tip of a wedge. Simultaneously, the spatial extend of this boundary layer around the tip shrinks like ε^2 . It thus follows that the wedge contribution to (9) will be $\mathcal{O}(\varepsilon^2\varepsilon^{n+1}\varepsilon^{n-1}) = \mathcal{O}(\varepsilon^{2+2n})$, which yields the result (2), (3). Achdou & Avellaneda [1] used (5), which is perfectly justified as long as the integration is performed over the entire pore volume consisting of boundary layer and perturbed bulk flow. The former contribution is $\mathcal{O}(\varepsilon^2\varepsilon^{n+1}) = \mathcal{O}(\varepsilon^{n+3})$, and they obtain the relation $w = 1 + \pi/(2\pi - \gamma)$

between the exponent w in (2) and the apex angle γ . The perturbed bulk potential flow should also be taken into account, however, and it happens that it is now a dominant contribution.

Numerical Computations

Numerical computations of the fields $\tilde{\mathbf{v}}$ and \mathbf{E} were performed for the periodic geometry depicted in Fig. 1. The values for the apex angle γ and the wedge height h were varied. The Stokes problem was solved using the variational formulation of the problem and a N_1 Finite-Element code based on a Uzawa decomposition method. To ensure accuracy, we have used an iterative automatic method, i.e., the solution is computed on the N_1 mesh, next an a-posteriori estimate of the error is computed, and finally the mesh is locally refined accordingly by means of a Delaunay technique developed by Rebay [8]. Successful use of this refinement method on sharp-edged wedges was reported by Firdaouss et al. [5]. Once the flow field is known, the dynamic permeability is computed using (1). Coherent computations of the potential field \mathbf{E} and the parameters (7), (17) were obtained using either the Schwartz-Christoffel transformation technique [3], or the method by [5]. From (2) it follows that the real part of the dynamic permeability should satisfy in the high-frequency limit, $\text{Re}\{k(\omega)\}/\delta^3 = A + B_w\delta^{w-1}$, where the constant A is related to the formation factor α_∞/ϕ and inverse length C , and the constant B_w is related to w , C_w , and the formation factor. The values of A , B_w , and w can be obtained by comparison between the high-frequency numerical data for $\text{Re}\{k(\omega)\}/\delta^3$ and the above theoretical form.

As an example, we show in Fig. 2 the results obtained for the exponent w when the wedge angle γ varies between 0 and $\pi/2$. The wedge height h is set 0.5. In the singular limit of knife-edge intrusions ($\gamma = 0$), the value $w = 1$ indicates the merging of the different terms. For flat surfaces $\gamma = \pi$, the value $w = 2$ will be obtained. The computed data are relatively close to the theory, the Achdou & Avellaneda predictions being plotted for comparison. As compared to the situation in smooth pore channels, the effect of sharp wedges is to produce a much slower convergence of the high-frequency dynamic permeability with respect to the Johnson et al. [6] development (1). In these situations, the development (2) does a much better job.

Summary

Analyzing in detail the fluid velocity patterns in oscillating tube flow, we have provided a new derivation of the Johnson et al. high-frequency development [6] and a new expression of the characteristic length Λ . Two different contributions to the dynamic permeability are now apparent. One stems from the boundary layer; another stems from a perturbation potential flow in the

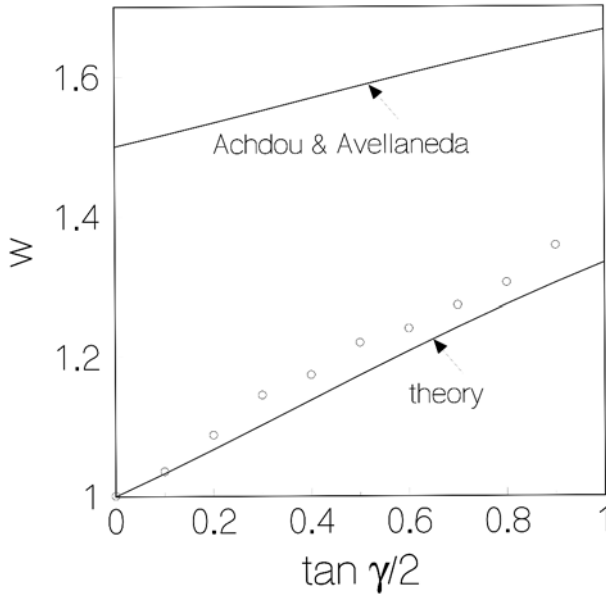


Figure 2. Dependence of the exponent w on the wedge apex angle γ for $h = 0.5$. The circles represent the numerical computations.

bulk, induced by the presence of the boundary layer. This understanding was applied to derive the correct form of the leading higher-order terms for sharp-edged geometries. Numerical computations substantiated this derivation.

References

- [1] Achdou, Y. and Avellaneda, M. (1992) Influence of pore roughness and poresize dispersion in estimating the permeability of a porous medium from electrical measurements, *Phys Fluids* **4** (12), 2561
- [2] Auriault, J.-L., Borne, L. and Chambon, R. (1985) Dynamics of porous saturated media, checking of the generalized law of Darcy, *J. Acous. Soc. Am.* **77**, 1641
- [3] Cortis, A. and Smeulders, D.M.J. (2001) On the viscous length scale of wedged shaped porous media, *Int. J. Engng Sci.* **235**, 307
- [4] Cortis, A., Smeulders, D.M.J., Guermont, J.-L. and Lafarge, D. (2003) Influence of pore roughness on high-frequency permeability, *Phys. Fluids* **15**, In press
- [5] Firdaouss, M., Guermont, J.-L. and Lafarge, D. (1998) Some remarks on the acoustic parameters of sharp edged porous media, *Int. J. Engng Sci.* **36**, 1035
- [6] Johnson, D.L., Koplik, J. and Dashen, R. (1987) Theory of dynamic permeability and tortuosity in fluidsaturated porous media, *J. Fluid Mech.* **176**, 379
- [7] Landau, L.D. and Lifschitz, E.M. (1959) *Fluid Mechanics*
- [8] Rebay, S. (1993) Efficient unstructured mesh generation by means of Delaunay triangulation and Bowyer-Watson algorithm, *J. Comp. Phys.* **106** (1), 125

- [9] Sheng, P. and Zhou, M. (1988) Dynamic permeability in porous media, *Phys. Rev. Lett.* **61** (14), 1591
- [10] Smeulders, D.M.J., Eggels, R.L.G.M and Van Dongen, M.E.H. (1992) Dynamic permeability: reformulation of theory and new experimental data, *J. Fluid Mech.* **245**, 211